

MODELS OF THERMAL PROCESSES FOR DESIGN OPTIMIZATION OF POWER PLANTS BASED ON RENEWABLE ENERGY SOURCES AND FUEL CELLS

by

**Alexander S. GRIGORIEV^a, Vladimir V. SKORLYGIN^a,
and Sergey A. GRIGORIEV^{b*}**

^a National Research Center "Kurchatov Institute", Moscow, Russia

^b National Research University "Moscow Power Engineering Institute", Moscow, Russia

Original scientific paper

<https://doi.org/10.2298/TSCI180710281G>

The system of mathematical models of thermal processes in hybrid power plants based on solar and wind renewable energy sources and methanol fuel cell has been developed to be used for the power plant design parameters optimization. Main assumptions and main equations for the heat and mass exchange in power plant are presented, methods and verification results for the power plant operation are given. Power plant design optimization and operation modes are discussed as well as experimental data collected during power plant operation. Forecast example for temperature fields during low ambient temperature operation is shown.

Key words: *stand-alone hybrid power system, mathematical model, heat and mass transfer, direct methanol fuel cell, renewable energy sources*

Introduction

There is a great demand for the autonomous hybrid power plants (HPP) with the capacity of about several kilowatts. Such power plants could be used for the development of North Regions in countries like Russia, Norway, Sweden, Finland, Denmark, Iceland, USA, and Canada. The HPP combine RES and fuel cells have to cover the lack of RES during polar night or emergencies. Design and optimization of such HPP require mathematical modelling of thermal and electrochemical processes, setting and completing of the corresponding calculative experiments. Although there is a lot of attention in the world to this modelling [1-3], specific features of north climate require more detailed study of thermal processes in HPP.

There are plenty of commercial software packages suitable for heat and mass exchange processes modelling [4-7], and a lot of experience of such application is collected. Nevertheless, besides the particular data for the temperature, flowrates and other data, developer of mathematical model of HPP needs the possibility to study all relationships between physical processes in HPP, and the study of heat processes is only a part of the general mathematical model for HPP. That's why it was decided to develop an own model for the thermal processes in HPP. This article presents main parameters of the mathematical models developed, as well as examples of these models application with experimental data for HPP tests in winter time.

* Corresponding author, e-mail: sergey.grigoriev@outlook.com

Autonomous HPP with solar panels, wind turbine and electrochemical system and its optimization problems

Application areas for HPP are the power supply of different consumers, such as telecommunication and mobile phone network as well as electric vehicle charging. Output power can vary from several Watts in the idle mode and up to 60 kW during fast charge of electric vehicle. Maximum energy output for HPP is 30 kW/h and is which may last 30 min for consumption. Main elements of HPP and their parameters are given in [8].

The power plant includes two blocks – a hardware container, C, and a wind power unit, W, (hereinafter referred to as *wind turbines*) installed on separate mounting bases, see fig. 1. The hardware container, fig. 1, includes the container unit C1 and the inside of the instrument cabinet, C2, with electronic equipment and a battery. Solar panels are mounted on the roof of the container unit. The container unit is divided with a partition wall and door, D2, into two parts – a vestibule, R1, and hardware compartment, R2. The hardware compartment and the instrument cabinet are equipped with automatic ventilation valves, V1 and V2, to avoid overheating of the equipment in summer. The design of the unit provides a temperature regime and protection from adverse climatic and man-caused impacts, as well as staff access for inspection and maintenance of HPP in both summer and winter seasons. Electronic devices inside the cabinet are, in addition to the payload components, the necessary controllers, a DC-DC converter, the control and monitoring system.

Front view of C2 is given in fig. 2.



Figure 1. The HPP front view and layout;

C – container, *W* – wind turbine, *C1* – equipment shelter, *C2* – cabinet; *D1*, *D2* – doors, *V1*, *V2* – vent valves, *R1* – air lock, *R2* – instrument room

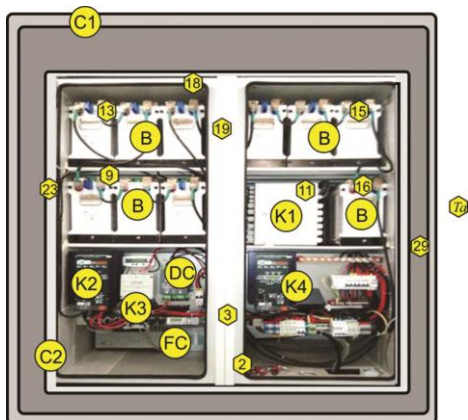


Figure 2. Front section of container and layout of the test set of temperature sensors;

B – battery units, *C1* – device container, *C2* – instrument cabinet, *K1* – *K4* – controllers, *FC* – fuel cell with fuel tank, 2 – 29 – temperature measurement points

The goals for the design of the previously mentioned capacity are:

- selection of optimal design and proper parameters for electronic devices to reach target consumption cycle under the following conditions: ambient temperature from $-50\text{ }^{\circ}\text{C}$ to $+45\text{ }^{\circ}\text{C}$, insolation variations from 1.5 months polar night to polar day, temperature limitations of the electronic devices and batteries, weight and size of the whole power plant.
- methanol consumption minimization.

The proper tools to reach these goals are multivariate calculations with codes that utilize mathematical models of stationary and non-stationary heat and mass exchange, electrochemical processes of energy generation and storage. The topic of this study is the description of mathematical models of thermal processes and the use of them for optimization tasks.

Mathematical models of thermal processes

Model of steady-state heat transfer

Common practice for analysis of heat and mass exchange processes is the use of steady-state heat transfer model. Mathematical model briefly described below is designed to solve the problem of heat conduction in 3-D approximation, therefore the container (being rectangular parallelepiped) was divided into the mesh of $L \times M \times N$ cells. The following conditions are valid for each cell: the thermal conductivity and volumetric heat dissipation are constant over the volume of the cell; the change in linear dimensions (thermal expansion) can be neglected.

For each cell, the Fourier law was written [9]:

$$\mathbf{q} = -\lambda \nabla T \quad (1)$$

The temperature gradient was approximated by a linear dependence. The resulting system of $L \times M \times N$ linear algebraic equations was solved either by the Gauss-Jordan method, or, for large dimensions, by the Seidel method [10]. Verification of the obtained code was carried out by constructing a model problem and comparing the results of the numerical solution with the analytical one [9].

The calculation code implementing the described method was widely used in the design of the HPP (see section *Application of the developed mathematical models*).

Model of thermal transients

Models and methods for calculating the steady-state temperature field [9, 11] are the standards for the design of buildings and structures, since they give certain *limiting* values of temperatures, which are subsequently compared with the normative ones. However, for the case of optimizing the design and parameters of uninhabited structures, estimates for stationary parameters are excessively conservative, especially since the stationary state of non-serviced HPP is not achieved in practice because of:

- daily and seasonal variations of ambient temperature and insolation,
- stochastic character of solar and wind generation, and
- the significant thermal inertia of a battery pack weighing up to 3000 kg, a cabinet, an instrument container weighing up to 4000 kg, where the characteristic heating/cooling times are several days and in their extent are comparable with the daily and weekly fluctuations of the ambient temperature.

The presented mathematical model was developed under the following assumptions, based on the accumulated experience [12], the results of the previous sections and the mass-dimensional characteristics of the equipment:

- each element of the cabinet (excluding the structural elements of the cabinet itself) is characterized by its unique boundary temperature and its 1-D spatial distribution (a more accurate 3-D distribution in the steady-state regime can be obtained from the stationary calculations of section *Model of steady-state heat transfer*, according to which, in our case, the maximum difference in the boundary temperatures does not exceed 1.5 °C),
- the flow of natural convection is considered to be lifted when flowing over an element with a higher temperature (the authors realize that this assumption in general might be not quite correct but detailed calculation we have for mass and dimensional characteristics of the described power plant is quite acceptable without substantial losses of the calculation speed), and
- the stabilization time of the air temperature along the wall is neglected.

The calculation scheme reproduces the construction of fig. 2, in which the following elements are marked with numbers: floor and ceiling of the cabinet 2 and 18 and container 36 and 39, the air cavity of the container from below 1, from above 30, from the right 29 and from the left 24, the air cavity of the cabinet from below 3 and from above 19, middle 9 and 16 and top 13 and 15 – left and right rows of batteries, software and hardware complex 11, controllers 6, 8 and DC-DC converter 7, left and right walls of container 35, the left and right walls of the cabinet – 3 points in height in each (31, 28, 33, 32, 28, 34), the fuel cell 40, the W_{sol} – heat flux of insolation on the roof, the T_a is the temperature of the outside air, the T_{ground} is the temperature of the bottom of the container.

The dynamics of thermal processes in the accepted assumptions is described by a system of ODE of conservation of energy. The total amount of incoming (outcoming) heat is calculated on the basis of eq. (1) as a sum along three axes:

$$Q(x_i, y_j, z_k) = Q_i^x + Q_j^y + Q_k^z \quad (1)$$

where for the transfer of heat by thermal conductivity, in all cases the linear approximation of eq. (1) is used, for example, for the axis $0x$:

$$Q_i^x = -\lambda_{ijk} F_{ijk}^x \frac{T(x_{i+1}, y_j, z_k) - T(x_i, y_j, z_k)}{x_{i+1} - x_i} \quad (2)$$

Then for the roof of the container 39:

$$\frac{dT_{39}}{dt} = \frac{1}{M_{39}C_{39}} (W_{sol} + Q_{3539} + Q_{3039} - Q_{3900}) \quad (3)$$

$$Q_{3539} = \frac{2\lambda_{35}F_{35}^z}{h_{35}} (T_{35} - T_{39}), \quad Q_{3039} = \frac{2F_{39}^z}{\frac{h_{30}}{\lambda_{30}} + \frac{h_{39}}{\lambda_{39}}} (T_{30} - T_{39}) \quad (4)$$

The Q_{3039} is calculated similar to Q_{3539} .

Equations for the remaining elements of fig. 2, excluding massive rechargeable batteries, are recorded in a similar way.

The following balance ratios are used for rechargeable batteries:

$$\frac{d\mathcal{G}_k^1}{dt} = \frac{1}{M_k^1 C_k^1} 2 \frac{\lambda_k^1}{d_k^1} \left[F_k^1 (T_k^1 - \mathcal{G}_k^1) - F_k^2 (\mathcal{G}_k^1 - T_k^2) + P_k^1 \right] \quad (5)$$

$$\frac{d\mathcal{G}_k^M}{dt} = \frac{1}{M_k^M C_k^M} \left[2 \frac{\lambda_k^M}{d_k^M} F_k^M (T_k^M - \mathcal{G}_k^M) + P_k^M \right] \quad (6)$$

where \mathcal{G}_k^p is the temperature of p^{th} layer, T_k^p – the temperature of p^{th} layer, C_k^p – the specific heat of p^{th} layer, P_k^p – the released power of p^{th} layer, M_k^p – the weight of p^{th} layer, F_k^p – the outer surface area of p^{th} layer, F_k^{p+1} – the inner surface area of p^{th} layer, λ_k^p – the coefficient of thermal conductivity of p^{th} layer, and d_k^p – the equivalent layer thickness of p^{th} layer.

For the linear channel streamed by the air-flow, the calculation scheme of fig. 3 is applied. The energy equation is integrated analytically, as a result of which the temperatures at the outlet of the slit and the total amount of heat are described by the relations

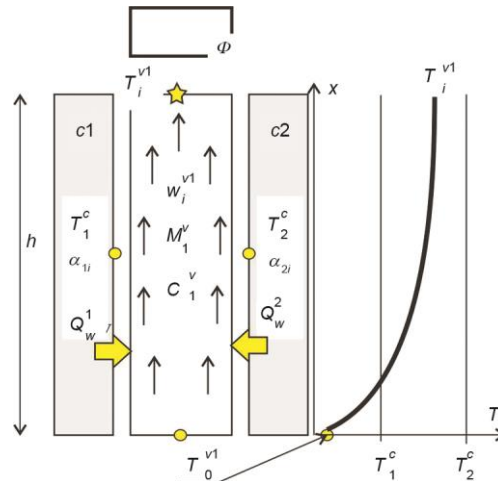


Figure 3. The calculation scheme for the air-flow channel

$$T_i^{v1} = \frac{a_1 T_1^c + a_2 T_2^c}{a_1 + a_2} + \left(T_i^{v0} - \frac{a_1 T_1^c + a_2 T_2^c}{a_1 + a_2} \right) \exp\{-(a_1 + a_2)x\} \quad (7)$$

$$Q_{w1(2)} = \alpha_{1(2)i} \Phi \left(T_{1(2)}^c - \frac{b}{g} \right) + \frac{\alpha_{1(2)i} \Phi}{gh} \left(T_i^{v0} - \frac{b}{g} \right) (e^{-gh} - 1) \quad (8)$$

$$a_1 = \frac{\Phi \alpha_{1i}}{M_1^v C_1^v w_i^{v1}}, \quad a_2 = \frac{\Phi \alpha_{2i}}{M_1^v C_1^v w_i^{v1}}, \quad \frac{b}{g} = a_1 T_1^c + a_2 T_2^c \quad (9)$$

The flow velocity, w , is calculated in advance using the methods described in [13] or, if the fuel cell is turned on, is known from its technical data. Then, for the element washed by the air flow, for example, for the middle part of the instrument cabinet:

$$\frac{dT_{28}}{dt} = \frac{1}{M_{28}C_{28}}(Q_{1628} + Q_{3228} + Q_{3428} - Q_{2829} - Q_{28}^c) \quad (10)$$

$$Q_{3539} = \frac{2\lambda_{35}F_{35}^z}{h_{35}}(T_{35} - T_{39}), \quad Q_{3039} = \frac{2F_{39}^z}{\frac{h_{30}}{\lambda_{30}} + \frac{h_{39}}{\lambda_{39}}}(T_{30} - T_{39}) \quad (11)$$

The Q_{1628} , Q_{3228} , and Q_{2829} are calculated by analogy with eq. (11), and for Q_{28}^c eq (8) is used. The remaining elements of the design scheme are described by equations of a similar structure except for the massive battery packs for which the design scheme eq. (6) was applied. The number of M layers varied from 2 to 8 (note that this did not affect the accuracy or performance of the code).

The fuel cell is modeled by an isothermal *black box* that converts the fuel of a predetermined G_{fuel} flow into electricity and heat [14]. The generated electricity is a source of heat in the controllers, DC-DC converters and chargeable batteries, unconverted energy during the operation of the fuel cell is converted into heat released by the operating fuel cell inside the fuel cell, P_{air} – heat carried away by air into the container and heat P_{water} – carried by hot water away from container, the amount of this water is known, see fig. 4.

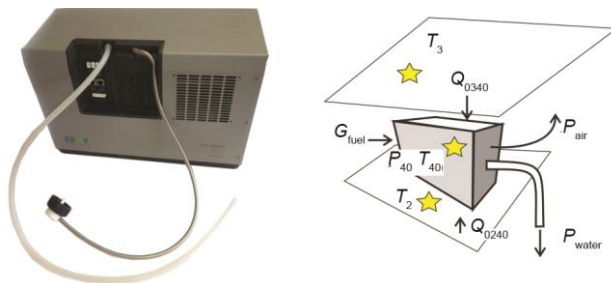


Figure 4. Fuel cell and its calculation scheme

The Q_{0240} , Q_{0340} – by analogy with eq. (11), t_0 is the moment of switching on, Δt – the warm-up time after switching on, T_{40}^{min} – the minimum temperature of fuel cell switching on is technical data, as well as heat removal P_{air} by air with air consumption G_{air} .

And for air cavity No 3 (between the cabinet floor and controllers, see fig. 2):

$$\frac{dT_3}{dt} = \frac{G_{\text{air}}}{M_3}(T_2 - T_3) + \frac{1}{M_3C_3}(Q_{3303} + Q_{3403} + P_{\text{air}}) \quad (12)$$

The system of eqs. (3)-(12) with boundary conditions of the first kind and relations similar to eq. (8) and eq. (11) is integrated by the second-order Runge-Kutta method [10].

The perturbing parameters are: ambient air temperature, soil temperature if the container is embedded in the foundation, the flux of solar radiation on the roof of the container, current charge, current payload, and fuel consumption in fuel cell. The last three parameters have a critical effect on the heat dissipation inside the instrument cabinet, and therefore, on the calculation results.

Examples of using the developed mathematical model are described in Section *Application of the developed mathematical models*.

Experimental study of HPP with solar panels, wind turbine and fuel cell

As previously noted, compliance with the temperature limitations for equipment and components of the HPP (and for the Russian conditions – the guarantee of non-freezing during a long cold winter) with a minimum of consumption of the consumed fuel cell and fuel is a criterion for the effectiveness of the design solutions of the power plant. Therefore, the developers of the HPP paid special attention to the experimental study of thermal regimes in the winter.

A feature of these studies is the long duration of a single experiment, which must be carried out in conditions of low ambient temperature. The section presents the results of the two extreme operating modes of the plant – with consumer power supply exclusively due to the stored energy in the battery and with the power supply based on RES and the fuel cell. The experiments were carried out in the Arctic zone of Russia sequentially with the forecast of a general prolonged lowering of the ambient air temperature.

The temperature registration scheme is shown in fig. 2. The graphs show the values of the measured temperatures at the respective points of the HPP. The velocity field, w , of the air-flow inside the cabinet was calculated in advance, the speed range was 0.005-0.07 m/s with corresponding range of the film coefficient, α , of 1-8 W/m²K.

Experiment with generating systems switched off

In this experiment, the most stringent possible thermal conditions are modeled – the idling power of the DC-DC converter is the only one source of internal heat generation. Time course of the characteristic temperatures are shown in fig. 5. The special value of this experiment is that it makes it possible to estimate the accuracy of the presented model of the dynamics of thermal processes; the maximum modulus deviation is taken as the measure of accuracy $\Delta y_{\text{mod}} = \text{Max}\{|y_e(t) - y(t)|\}; t \in [t_1; t_2]$.

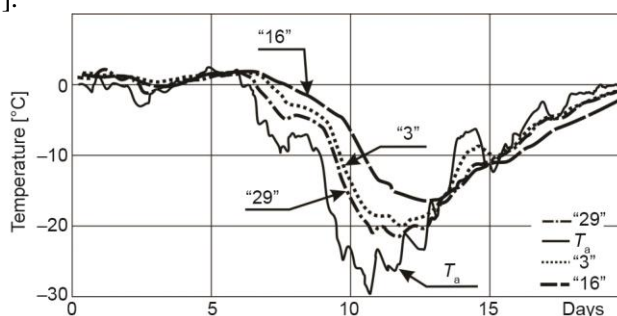


Figure 5. Time course of temperature of power plant with generation systems switched off

The minimum temperature of the HPP elements (1st column) and its delay (2nd column) in comparison with the temperature of ambient air is summarized in tab. 1. The deviation of the measured values from the calculated test data are also given there (3rd column).

One could see that the represented design of the power plant provides a suitable temperature regime even with a minimum heat release (2-4 W in the enclosure volume): the lowest temperature of electronic devices is -16.8 °C, and the lowest temperature of battery is -20.9 °C even with the outside temperature dropping to -29.7 °C. This (worst) mode of op-

eration have lowest probability in real operation, therefore the presented experimental data are very important for assessing the quality of the HPP project.

Table 1 shows that the simple mathematical model has satisfactory accuracy for practice. In addition, the experiment once again confirmed the need to study thermal processes precisely in dynamics, from this point the importance of the development of mathematical models and calculation codes is quite obvious.

Table 1. The minimum temperature during the test, its delay in relation to the ambient air, and the maximum modulus deviation

Temperature measurement point	Lowest temperature, [°C]	Delay, [hours]	Maximum modulus deviation, [°C]
T_a – Ambient air (5 cm from the outer wall of container)	-29.8	0	
2 – Instrument cabinet floor	-21.5	13	2.3
3 – Air cavity at the cabinet bottom	-19.8	29	2.2
9 – Left middle row of batteries	-20.9	54	3.1
11 – Software and hardware complex	-16.8	53	2.9
13 – Upper left row of batteries	-16.5	54	3.0
15 – Upper right row of batteries	-16.5	54	2.9
16 – Right middle row of batteries	-16.5	29	3.2
18 – Instrument cabinet ceiling	-15.5	58	2.5
19 – Air cavity on top of cabinet	-16.1	55	2.7
23 – Left wall of instrument cabinet	-16.5	58	2.8
29 – Right wall of container	-21.1	4	2.1

Experiment with generation systems based on solar panels and fuel cells

Experiments were continued in conditions of constantly dropping temperature of the ambient air. Approximately one month after experiment previously described, fuel cell was added to the generation system. Temperature changes for the next 20 days are shown in fig. 6.

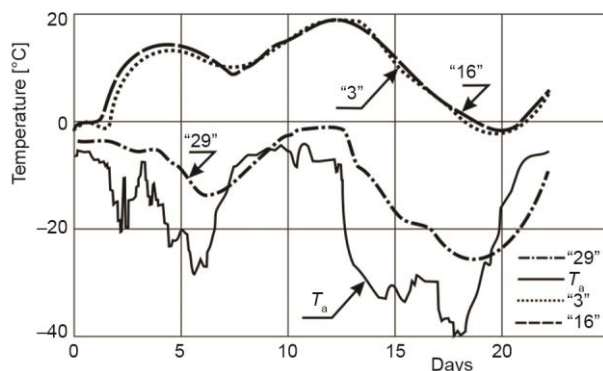


Figure 6. Time course of temperature of power plant with disconnected generation systems

Time course of the temperature for all elements inside instrument cabinet is approximately the same, temperature difference from each other is about 5 °C and the temperature variation is in the range from -5 °C to 20 °C.

A similar picture was observed throughout the operation of the plant until April. This proves the efficiency of the fuel cell not only as a tool for compensation for the energy deficit, but also as a way of the temperatures stabilization inside the instrument cabinet. The latter allows expanding the possible range of consumer equipment.

Application of the developed mathematical models

The developed system of mathematical models was used to develop and operate prototypes of HPP.

Optimization of instrument cabinet design

Development of the cabinet design could be presented as an example of the design optimization. Location of the devices upwards in the first version of the design was changed to the location downwards by results of multivariate calculations. The temperature field by volume was leveled; the location and geometry of the devices were corrected. Figure 7(a) shows initial, and 7(b) optimized versions of cabinet design. Final design of HPP, fig. 2, was done with the help of the optimization results previously given.

Calculated prognosis of operability at extremely low temperature

The main area of application of the dynamics models is the calculated forecasts of the temperature regime of the HPP in hypothetical extreme or emergency situations. Figure 8 shows the time course of the characteristic temperatures assuming a sudden drop in the temperature of the ambient air to -50 °C and the operation of the fuel cell according to the logic of section *Mathematical model of thermal processes* – starting at the temperature of the lower air cavity $T(3) = 2$ °C.

The fuel cell starts at point A, the temperature increases due to the accumulated heat. This heat is released during time $t_B - t_A \cong 50$ hours. At point B cooling begins. After about 10 days the temperature field is stabilized by the operation of the fuel cell.

The calculated forecast of the temperature field in the presence of a temperature stabilization system

The experimental data of figs. 5 and 6 show that input power regulation is advisable

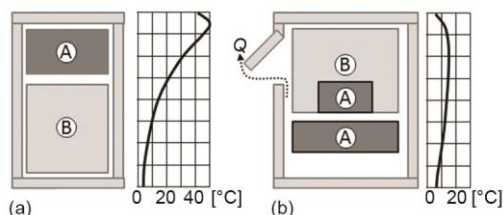


Figure 7. Temperature difference in height between the container wall and the cabinet with different design options;
 A – devices, B – chargeable battery,
 (a) – initial version, (b) – optimized version

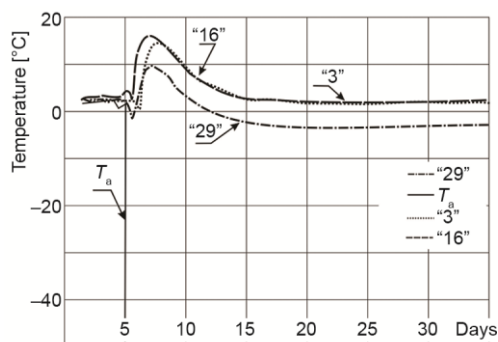


Figure 8. The calculated forecast of the characteristic temperatures of the HPP elements in winter when the temperature of the ambient air is hypothetically abruptly lowered from +2 °C to -50 °C

to get the constant temperature in the instrument cabinet. The simulation of the process, fig. 9, was carried out under the assumption of relay control of the heat supply to evaluate effectiveness of such temperature control. The fuel cell was switched on when temperature in the Point 3 of fig. 2 dropped down to $+2\text{ }^{\circ}\text{C}$ and switched off when temperature reached $+5\text{ }^{\circ}\text{C}$. Forecast shows that when the generated power is sufficient for customer supply, regulated heat supply could reduce the fuel cell and fuel consumption by 3-5 times compared to constant operation of fuel cell after the necessary temperature is reached for the whole volume of the instrument cabinet.

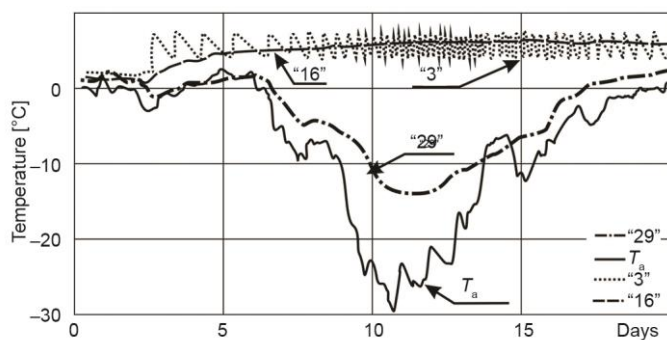


Figure 9. Simulation of the operation of a tracking system for supplying heat from a fuel cell

Assurance of the necessary temperatures in HPP with RES and fuel cell intended for use in north climate is one of the targets to be reached during design process. The authors used the following approach to save a lot of efforts and time for the design of the HPP: use of the basic set of energy equations for fast configuration and change of the calculation scheme and make a large series of variant calculations. This approach allowed completing the following tasks:

- optimize general design scheme *cabinet inside container*, determine specific sized under the limitations of the size and weight,
- optimize the layout of the equipment within the cabinet with the maximum use of air-flow with natural convection,
- optimize the control parameters of the controllers and the control logic when the generating sources work together on the load, and
- to justify operability under extreme weather conditions and possible emergency situations without carrying out costly climatic tests on a special stand.

Conclusions

Mathematical models of thermal processes were created to be applied for the design optimization and proof of the operability of hybrid power plants with RES and fuel cell in wide range of climate conditions.

Test results of the operating HPP were used for verification. Comparison shows that the model and code described in this article have acceptable accuracy (2° in amplitude and 3.5° by modulus). This is valid for devices whose temperatures were directly measured in the experiment and with certainty for the structural elements, because there is a good compliance between the calculated and measured temperatures of the air cavities of the container and the cabinet. Use of the developed models allowed determining main geometry and weight of HPP described in [8], optimize equipment location, evaluate physical parameters at extremely low temperatures, and develop suggestions for the modernization of HPP and its parameters.

The authors hope that the described modeling experience will be useful for developers of renewable energy plants, the number of which is constantly growing in the world.

Acknowledgment

Financial support from the Ministry of Science and Higher Education of the Russian Federation within the framework of agreement on granting No 14.604.21.0164 from 26.09.2017 (unique project identifier RFMEFI60417X0164) is acknowledged.

Nomenclature

C – specific heat, [$\text{Jkg}^{-1}\text{K}^{-1}$]
 d_{ik} – distance between surfaces of i^{th} and k^{th} elements along the y-axis, [m]
 F – surface area, respectively, for k^{th} elements in the planes Oyz , Oxz , Oxy , [m^2]
 h_{ik} – distance between surfaces of i^{th} and k^{th} elements along the axis Oz , [m]
 M – mass, [kg]
 P – power, [W]
 q – heat flux, [Wm^2K^{-1}]
 T, U – temperature, [K]
 T_a – temperature of ambient, [K]
 w – air velocity, [ms^{-1}]

Greek symbols

α, α_{ijk} – film coefficient, [$\text{Wm}^{-2}\text{K}^{-1}$];
coefficients in equations
 λ – heat conductivity, [$\text{Wm}^{-1}\text{K}^{-1}$];
 \mathcal{G} – temperature averaged over the layer, [K]
 Φ – slit surface area, [m^2]

Acronyms

B – battery
C – container
HPP – hybrid power plant

References

- [1] Bhandari, B., et al., Mathematical Modeling of Hybrid Renewable Energy System: A Review on Small Hydro-Solar-Wind Power Generation, *International Journal of Precision Engineering and Manufacturing-Green Technology*, 1 (2014), 2, pp. 157-173
- [2] Santos, S. F., et al., New Multi-Stage and Stochastic Mathematical Model for Maximizing RES Hosting Capacity // *IEEE Transactions on Sustainable Energy*, 8 (2017) 1, pp. 304-319
- [3] Nguyen, X. H, Nguyen, M. P., Mathematical Modeling of Photovoltaic Cell/Module/Arrays with Tags in Matlab/Simulink, *Environ Syst Res* 4 (2015), Dec., 24
- [4] ***, TRNSYS– Transient system Simulation Tool <http://www.trnsys.com/>
- [5] ***, Engineering Simulation & 3-D Design Software ANSYS. <http://www.ansys.com>
- [6] ***, COMSOL Multiphysics® Modeling Software. <https://www.comsol.com/>
- [7] ***, Simulink. Matlab. <https://matlab.ru/products/simulink>
- [8] Grigoriev, A. S., et al., A Hybrid Power Plant Based on Renewables and Electrochemical Energy Storage and Generation Systems for Decentralized Electricity Supply of the Northern Territories. *Int. J. of Electrochemical Science*, 13 (2018), 2, pp. 1822-1830
- [9] Eckert, E. R. G., Drake, R. M., *Analysis of Heat and Mass Transfer*, McGraw-Hill, New York, USA, 1972
- [10] Epperson, J. F., *An Introduction to Numerical Methods and Analysis* (2nd Edition), Wiley, New York, USA, 2014
- [11] Kusuda, T., Fundamentals of Building Heat Transfer Institute for Applied Technology *Journal of research of the National Bureau of Standards*, 82 (1977) 2, pp. 97-106
- [12] Ponomarev-Stepnoi, N. N., et al., Analysis of Critical Reactor Response for TOPAZ-II Water Immersion Scenarios, *Proceeding*, 11th Symposium on Space Nuclear Power and Propulsion, CONF-940101, American Institute of Physics, New York, USA, pp. 1069-1071
- [13] Roache, P. J., *Computational Fluid Dynamics*. Hermosa Publishers, Albuquerque, N. Mex., USA, 1976
- [14] Doucet, G., Etievant, C., et al., Hydrogen-Based PEM Auxiliary Power Unit, *International Journal of Hydrogen Energy* 34 (2009) 11, pp. 4983-4989